**THE EUROPEAN
PHYSICAL JOURNAL D**

Regular Article

Simulation of electrical discharge in a 3.6 Joule miniature plasma focus device using SIMULINK

Hossein Jafari and Morteza Habibi[a]

Department of Energy Engineering and Physics, Amirkabir University of Technology, Tehran, Iran

Abstract. A novel technique has been developed and studied in this paper to simulate the electrical discharge circuit of a 3.6 J miniature plasma focus device (PFD) and investigate the effect of inductance variation on voltage spike and current dip. The technique is based on a correlation between the electrical discharge circuit and plasma dynamics in a very small PFD that operates at the energy of 3.6 J. The simulation inputs include the charging voltage, capacitor bank capacitance, current limiter resistance, by-pass resistance as well as the time-dependent inductance and resistance of the plasma sheath which are calculated by assuming the plasma dynamics as transit times in going from one phase to the next. The variations of the most important elements in the circuit (i.e. the constant and breakdown inductances) and their effects on the current dip are studied in PFDs with low and high constant inductance. The model demonstrated for achieving a good pinch in the PFD, although the total inductance of the system should be low; however there is always an optimum inductance which causes an appropriate pinch. Furthermore, the electrical power produced by the pulsed power supply, the mechanical energy as well as the magnetic energy which are transferred into the plasma tube were obtained from simulation. The graph of electrical power demonstrated a high instantaneous increment in the power transferred into the plasma as one of the greatest advantages of the pulsed power supply. The simulation was performed using software tools within the MATLAB/SIMULINK simulation environment.

1 Introduction

A dense plasma focus device (PFD) is a well-known intense pulsed source of energetic beams, as discovered by Filippov et al. [1] and Mather [2]. The PFD is able to produce short-lived pinched plasma ($\sim$100 ns) that is sufficiently hot ($\sim$1 keV) and dense ($\sim10^{20}$ cm^{-3}) to enhance nuclear fusion reactions [3]. This device essentially consists of two coaxial electrodes located inside the chamber that is filled with gas at low pressure. The inner electrode is anode which is electrically insulated from the outer electrode by a coaxial insulator. By discharging a capacitor bank, a pulsed high voltage is induced across the electrodes, generating a uniform surface of plasma across the insulator. The created plasma is accelerated by the Lorentz force to form pinched plasma at the open end of electrodes. The pinch produces energetic pulses of neutron beams (using deuterium as the operating gas), electron beams, and X-ray emissions. There are many remarkable efforts and researches that have invested in PFDs with various ranges from a few tens of joules to mega joules [4,5]. The PFD, generating neutrons in the range of 10^6 to

10^{10} neutrons per pulse will have substantial use in the physics and engineering applications [3,6–13]. The PFD with a very low range of energy and a shorter physics processes is capable to work in a repetitive regime from Hz to kHz and its being as a compact, portable and safer device is very noteworthy in engineering applications such as substance detection, X-ray imaging, microlithography, oil humidity measurements, medical neutron therapies, and etc. The following recent works indicate the extension of the small PFDs for various potential applications. Evidence of pinching has been observed on electrical signals at 60 mJ nanofocus [14] which expected to yield about 10^3 neutron per pulse for discharges operating in deuterium at 10 kA. The battery (12 V dc, 400 A h) powered transportable PFD with its capacitor bank that is charged up to 125 J and discharged at just 30% has been reported [9] to generate 10^5 to 4×10^6 neutrons per pulse. The battery (24 V dc, 7.5 A) powered miniature PFD, having a single capacitor (200 J, 4.0 μF, 10 nH) has been reported [15] in which the average yield of neutron is $(1.6 \pm 0.3)\times10^6$ neutron/shot in 4πsr with a pulse width of 23.4 ± 3.3 ns for the first 50 shots. The 400 J fast PFD has been reported [16] to produce $(1.06 \pm 0.13)\times10^6$ neutrons per shot at 9 mbar

^a e-mail: mortezahabibi@aut.ac.ir

deuterium gas pressure and a 30 kV charging voltage. The formation of pinch in the PFDs have also been reported at very low energies of 50 J [17], 50–70 J [18], 5–160 J [19], 32–102 J [20] and 100 J [21].

The main goal of this work is to simulate the electrical discharge circuit of a very compact and portable PFD as an intense pulsed source. Thus, a conceptual design is presented for a PFD with a 3.6 J bank of energy, charging via a very compact battery powered energy driver. Then, a novel technique is utilized for simulating the electrical discharge circuit of the device using the values obtained from the design as inputs of the simulation.

There are some studies and reports about effects of the electrical parameters of PFDs on the discharge voltage and discharge current signals. It has been reported [22–25] that there is in fact an optimum circuit inductance below which a pinch current limitation effect occurs indicating the neutron yield of PFD would not increase, despite of increasing the peak total current. It has been presented [26] that the plasma resistance at the pinch phase in very low energy devices is greater than those with larger energy that is because of the small diameters of both anode and insulator. This point should be considered during the modeling of the very small PFDs. It has been found [27] that PFDs with low circuit inductance have a regular current dip during the pinch phase, whereas those with high circuit inductance have an extended current dip beyond the regular current dip because of growing an anomalous resistance during and after the pinch phase.

In this paper, the effect of variation of parameters, particularly the inductance variation effects on the voltage spike and current dip in PFDs with low to high constant inductances are investigated. The optimum inductance of this device is also chosen by investigating the output signals.

2 Design considerations

The design process of a PFD is begun considering the principal electrical parameters. The PFD designed here is of a Mather type configuration [28] which is energized by a capacitor bank (32 nF, 15 kV, 3.6 J) consisting of four ceramic capacitors (8 nF, 5 nH). The capacitor bank is charged up to 15 kV by means of a switching power supply which is energized with a rechargeable battery (12 V dc, 20 A h). The device dimensions are obtained using the two essential parameters introduced in the well-known models in the design of PFDs [4,29], i.e. the energy density parameter ($28E/a^3$, where E is the energy of capacitor bank and a is anode radius) and drive parameter ($S = I_0/a\sqrt{\rho}$, where I_0 is discharge current, and ρ is mass density), so that they become compatible with very small PFDs. The energy density parameter indicates to the amount of discharge energy transferred to the total plasma volume. Then, whatever it is greater, it causes to increase the energy of electrical carriers in the plasma, producing more energetic neutrons and X-ray emissions. However, the drive parameter constrains an optimum value for it because the energy density parameter

is actually proportional to $S^2\rho$ [30]. The drive parameter plays an important role to transfer the magnetic energy per unit mass of plasma ($\sim S^2$). Every increment of it will lead to an increase in the kinetic energy ($\sim S^2$) and speed ($\sim S$) of the plasma sheath. Hence, the thermal energy per unit mass of plasma sheath will be increased. This high thermal energy enhances temperature of the fusion reactions (beam-target and thermonuclear fusion reactions) which causes to emit more neutrons. By assessing the small PFDs constructed in the range of energy less than 100 J operating in deuterium [14,17–21] the energy density parameter and drive parameter are decided to be 5×10^{10} J/m^3 and 70 kA/cm torr$^{1/2}$, respectively. Due to this energy density, the anode radius is calculated to be 1.263 mm. The total inductance of the designed device is expected to be about 60 nH that leads to the discharge current of 10.95 kA. Thus, concerning to the drive parameter of 70 kA/cm torr$^{1/2}$, the suitable operating pressure of deuterium is obtained around 1.5 torr to have a good ionization over the insulator. In order to obtain the effective anode length, the first quarter of the discharge period that has been calculated to be 68.82 ns must be coincident with the moment of the pinch. In this case, the first quarter-period is introduced as sum of durations of the breakdown, axial acceleration and radial phases, i.e. we can use the relation of $T/4 = t_b r + (z_a/v_a) + (a/v_r)$ to calculate the effective anode length.

The breakdown phase duration is dependent on the initial gas condition, effective insulator length and dimensions of electrodes [31,32]. It has been reported [31–33] that reduction of the operating gas pressure leads to increase the breakdown phase duration. It should be mentioned that increasing the insulator length causes the gliding discharge to occur in the lower pressures [34], then the effective insulator length should be determined so that these two points are considered. On the other hand, much investigations devoted to the small PFDs show that duration of the breakdown phase can assign values from 15% to 30% of the quarter-period of the discharge [3,19,26,35], whereas those devices operated with charging voltages of 10 to 38 kV and the effective insulator lengths of 5 to 20 mm as optimum effective lengths of insulator. Hence, concerning to the low operating pressure of 1.5 torr gas deuterium and charging voltage of 15 kV, we decide to use an effective insulator with a length of 13 mm (with outer radius of 4 mm) and consider a time about 25% of the quarter-period of the discharge (i.e. about 17 ns) into account for the breakdown phase. As a result, regarding to the axial and radial speeds of plasma sheath (of the order of $(0.8 - 1) \times 10^5$ m/s and $(1.5 - 2.5) \times 10^5$ m/s, respectively) [14], the effective anode length is obtained to be about 4.53 mm. In order to estimate the cathode radius, it should be attended that the length of the insulator should be greater than distance between electrodes, because if the distance between electrodes becomes greater than the insulator length, the sliding discharge will not only develop along the insulator that is due to the surface capacitance effect [31,36], but also a radial discharge will develop between the electrodes [37]. This event may cause to form an

Table 1. The main electrical and geometrical characteristics of several small PFDs.

Reference	W_0 (J)	V_0 (kV)	a (mm)	b (mm)	z_a (mm)	L_{ins} (mm)	L (nH)	$\tau/4$ (ns)	$\frac{l_{ins}}{b-a}$	$\frac{b}{a}$
Silva [16]	400	30	6	13	7	14	38	300	2	2.16
Rishi [39]	200	30	4	11	20	5	32.9	370	0.714	2.75
Rout [15]	200	10	5	17	20	12	46	675	1	3.5
Rishi [39]	170−270	12−15	6	15	17	5	27	400	0.556	2.5
Beg [13]	100	38	10	22.5	30	20	−	800	1.6	2.25
Hassan [19]	58−160	30	9.5−6.5	24	7	14.6	53	325	1.007	3.69
Patricio [18]	32−98	20−35	6	13.5	5	5	65	220	0.667	2.25
Soto [40]	50	25−30	3	11	4.8	19.2	38	150	2.4	3.67
Soto [41]	0.1	5−10	0.22−0.8	−	0.4	10	5	16	−	−

Table 2. The electrical and geometrical parameters of the system.

Symbol	Parameter	Value
V	Operating voltage (kV)	15
C_0	Capacitor bank capacitance (nF)	32
E	Capacitor bank energy (J)	3.6
I_0	Peak discharge current (kA)	10.95
L	Total inductance (nH)	60
$T/4$	Quarter period (ns)	68.82
$28E/a^3$	Energy density parameter (J/m^3)	5×10^{10}
S	Drive parameter (kA/cm torr$^{1/2}$)	70
a	Anode radius (mm)	1.263
z_a	Effective anode length (mm)	4.53
b	Cathode radius (mm)	7.17
P	Operating gas pressure (torr)	1.5
l_{ins}	Effective insulator length (mm)	13
SS304	Anode material	Stainless steel
SS304	Cathode material	Stainless steel
	Insulator material	Pyrex

Fig. 1. Equivalent electrical circuit of the PF discharge [31].

3 Modeling of discharge circuit

To simulate a discharge circuit in a PFD, it is necessary to know the precise relation between various phases of the plasma dynamic and equivalent electrical circuit. Figure 1 shows the equivalent circuit of the PFD, where C_0 is capacitance of the capacitor bank; R_0 and L_0 are the resistance and inductance of the capacitor bank, transmission line and connections, and spark gap switch, respectively; L_p and R_p are the time-dependent inductance and resistance of the plasma sheath respectively which theirs values depend on the position occupied at each moment along the electrodes.

The most important parameter of the discharge circuit is inductance which changes with the phases of plasma dynamics. The system inductance is particularly composed of constant inductance (includes inductances of the capacitor bank, spark gap switch, and connections between them) and variable inductance (includes inductances of chamber and plasma). For achieving a suitable pinch, the constant inductance should be very low. Therefore, the structure of vacuum chamber, spark gap, capacitor bank, and their connections are designed in a very compact state. In our design, the constant inductance is expected to be of the order of 30 nH. The total inductance for this device is estimated to be about 60 nH. The plasma motion causes the plasma dynamics to have several phases with their own inductances from one phase

inappropriate discharge into the tube, leading not to produce a good pinch. For taking into account the point, it can be used an empirical scaling parameter that is defined as $l_{ins}/(b-a)$ [37], because this parameter has a constant order for small and large PFDs. Table 1 shows the main electrical and geometrical characteristics of several small PFDs. As shown in Table 1, the parameter of $l_{ins}/(b-a)$ in the small PFDs can include the values from 0.556 to 2.4. Since the ratio between cathode radius and anode radius should be in a reasonable range [38], therefore we consider the scaling parameter of $l_{ins}/(b-a)$ to be about 2.2. Hence, concerning to the dimensions of anode and insulator, the cathode radius results in $b = 7.17$ mm. This cathode radius leads the parameter $C = b/a$ to be about less than 6. This value for a very small PFD can be reasonable because the anode radius of this device is very small. It should be mentioned that if we choose a small cathode radius, the distance between anode and cathode will be so small that it may cause to occur the improper breakdown. The electrical and geometrical parameters of the 3.6 J PFD are listed in Table 2.
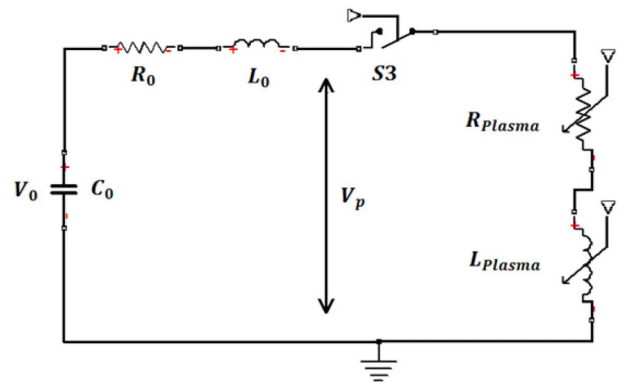
to the next. In general, the plasma dynamics is related to the discharge circuit of the PFD via five phases with titles of pre-breakdown, electrical breakdown, axial acceleration of plasma sheath, radial collapse (pinch phase), and expanded column axial phases [42]. With respect to the first quarter-period of 68.82 ns, the total duration of these phases is estimated at about 120 ns, so that the first 15 ns is for the pre-breakdown phase, and the remaining 105 ns is for the next phases. These durations along with the other physical parameters of the discharge circuit are applied into the simulation as input values. The variations of the plasma inductance are appeared in these phases as follows.

3.1 Pre-breakdown phase

It is found that only a fraction of the measurable discharge current actually flows through the plasma pinch, a phenomenon which is sometimes termed the current shedding effect [31]. Also, there is always a pre-breakdown voltage that is appeared in electrical signals, before the discharge occurs. Therefore, the equivalent circuit shown in Figure 1 should be modified by adding a parallel branch as a bypass impedance to fulfill both purposes mentioned above [43]. The by-pass impedance can be a resistor or an inductor. Although using the inductor instead of the resistor causes to produce a high pre-breakdown voltage with a shorter rise time, however, in order to avoid the inductive interference over the discharge signals, we prefer to use the resistor as the by-pass impedance. The by-pass resistance ($R_{\text{by-pass}}$) plays three roles in this circuit: (1) during the pre-breakdown phase, it is in parallel with capacitor as the equivalent series resistance (ESR). Thus, it represents losses in the capacitor; (2) it is also used for sampling the pre-breakdown voltage across the electrodes; and (3) during the breakdown phase and the next phases, it will become in parallel with plasma variable impedance as the leakage resistance. Therefore, after charging the capacitor bank up to the operating voltage, the capacitor should be separated from the main power supply. Then it is immediately connected across the by-pass impedance to induce a high voltage pulse across it. All switching processes of this phase are performed by two switches at the total duration of 15 ns as the time of pre-breakdown phase ($t_{\text{pre-breakdown}}$). It should be noted that if the duration of the pre-breakdown phase takes long time, regarding to the value of the by-pass resistance (ESR), the energy stored into the bank is lost without having any efficiency. Therefore, the $t_{\text{pre-breakdown}}$ should be chosen so that the losses become least. The $R_{\text{by-pass}}$ is obtained regarding to the fraction of discharge current that is flowed through the plasma impedance. The current factor (f_c) in large devices can be in the range of 0.7 to 0.9 [44–46] but in small devices, the current factor is lower [39] because of having the small electrodes. The by-pass resistance can be calculated using the characteristic impedance as follows:

$$R_{\text{by-pass}} \sim \frac{\sqrt{\frac{L_0}{C_0}}}{f_c}. \tag{1}$$

Hence, by assuming a current factor of 0.6, the by-pass resistance can be about 2.28 Ω. It is decided to investigate the by-pass resistance from 1 to 5 Ω in simulation as the input.

3.2 Breakdown phase

This phase includes processes of the electrical breakdown, plasma sheath formation and detachment from the insulator surface [26]. The electrical breakdown occurs by triggering the spark gap switch (S3) at the optimized operating pressure. Then a sliding discharge develops along the insulator because of the effect of the surface. The created plasma sheath remains attached along the insulator surface for a duration of the discharge until the sliding discharge reaches the end of the insulator. Hence, the anode is connected to the cathode and the plasma sheath is then detached and lifted off from the insulator surface by the Lorentz force [31]. As a result, in designing of a very small PFD, the duration of the breakdown phase ($t_{\text{breakdown}}$) plays a very important role because the anode length and finally the inductance of the tube will be estimated by taking into account this parameter. With respect to the quarter-period of 68.82 ns, it is calculated a duration about 10.32 to 20.6 ns for the breakdown phase to apply in simulation. It should be attended that the space ionized around the anode causes the electrical resistance of plasma suddenly to decreases. The plasma resistance during this phase ($R_{\text{breakdown}}$) can be calculated by relation that is given by:

$$R_{\text{breakdown}} = \eta_{\text{spitzer}} \frac{L_{\text{ins}}}{\pi(\Delta^2 + 2R_{\text{ins}}\Delta)} \tag{2}$$

where η_{spitzer}, R_{ins} and Δ are Spitzer's resistivity, outer radius of insulator sleeve and sheath thickness of plasma, respectively [26]. Regarding to the anode radius of 1.263 mm, the sheath thickness can have a value about 0.1 mm.

Applying the Spitzer' resistivity in relation (2) which is obtained with a 2 eV fully ionized deuterium plasma [26], the plasma resistance is calculated to be about 1.06 Ω. In this case, the plasma resistance that is studied in the simulation as Input has a value from 0.9 to 1.1 Ω.

The magnetic field produced by flowing the high electrical current through the created plasma and anode leads the plasma to have a small amount of inductance that is called $L_{\text{breakdown}}$. The $L_{\text{breakdown}}$ is estimated concerning to the part of inner electrode surrounded by the insulator sleeve and other connections like cathode and anode plates. The vacuum chamber of this device is designed such a way that the anode is connected to the spark gap switch directly. In this case, the total length of anode considering the anode and cathode plates and insulator between them is about 80 mm. Therefore, the $L_{\text{breakdown}}$ is calculated to be from 15 to 20 nH and applied into the simulation.

3.3 Axial acceleration phase

During the axial acceleration phase, the capacitor bank is discharging through the plasma sheath and electrodes. Therefore, immediately after formation of the thin plasma sheath, the magnetic forces cause the plasma to accelerate forward along the axis of the electrodes. In this case, by changing the position of the plasma sheath, the plasma inductance will change in accordance to the inductance formula in axial phase that is given by:

$$L_{\text{axial}} = \frac{\mu}{2\pi} z_a \ln \frac{b}{a} \tag{3}$$

where z_a, b, and a are the effective anode length, cathode radius, and anode radius respectively. Since the time intervals of different phases and also variation of plasma inductance are very small, it can then be assumed that the plasma has a behaviour like an inductor in which its value is linearly increasing in time from $L_{\text{breakdown}}$ up to L_{axial}. The variation of the plasma inductance during the axial acceleration phase can be estimated by equation (3) to be about from 1.5 to 2 nH. Regarding to the axial speed of plasma sheath, therefore the duration of the axial phase applied into the simulation is calculated to be in the range of 45.3 to 56.62 ns. In order to calculate the plasma resistance during the axial phase (R_{axial}), there is a relation that is defined as follows:

$$R_{\text{axial}} = \eta_{\text{spitzer}} \frac{\ln(r_{\text{out}}/r_{\text{in}})}{2\pi\Delta} \tag{4}$$

where r_{out} and r_{in} are outer and inner radius of plasma [26]. Hence, the radius of anode and cathode of the 3.6 J PFD lead to a plasma resistance of about 0.55 Ω. The plasma resistance that is investigated in simulation can be from 0.5 to 0.6 Ω.

3.4 Radial collapse (Pinch phase)

When the plasma sheath reaches the end of the electrodes, the open end of the anode prevents further progress of the plasma, and the $J \times B$ force causes the plasma to constrict, forming a highly dense hot plasma pinch with the minimum radius. During the pinching, the plasma is elongated toward the central axis so that it possesses a minimum radius and a long length. Under this situation, regarding the Spitzer's resistivity equation the plasma resistance increases in time so that its value will become maximum at the end of the phase [27]. It has been observed that the length and radius of the pinch are of the order of $z_{\text{pinch}} = 0.8a$ and $r_{\text{pinch}} = 0.12a$, respectively [26,29,41]. As a result, during the pinch phase, the plasma resistance (R_{pinch}) can be calculated by a formula as follows [26].

$$R_{\text{pinch}} = \eta_{\text{spitzer}} \frac{z_{\text{pinch}}}{\pi (r_{\text{pinch}})^2}. \tag{5}$$

Using relation (5), the pinch resistance is obtained to be about 0.9 Ω. Hence, the resistance that is applied into

the simulation is considered to be about 0.8 to 1 Ω. This plasma resistance is expected for the 3.6 J very small PFD since the dimensions of anode and its insulator as well as the sheath thickness in a very low energy devices are considerably lower than those in large energy devices. This anomalous plasma resistance at the radial phase would effect on the pinch stability and in high constant inductance systems is what causes the voltage spike and the current dip [26,27]. With respect to the radial speed of the plasma sheath, the radial phase duration can be estimated to be from 5.05 to 8.42 ns. The inductance of the pinch phase (L_{pinch}) is related to the magnetic permeability and dimensions of plasma column that are varying during the pinching. As the dimensions of the plasma column are proportional to the anode radius, the plasma inductance in the radial phase can be estimated to have a value from 1.5 to 2.5 nH. The increasing sharply the plasma inductance and growing the anomalous resistance during the radial phase would represent the plasma instabilities causing a dip on the discharge current. This current dip at the pinch phase is called the regular dip [27]. It is found that if a PFD with low constant inductance is modeled using the five-phase Lee model code it would have a big regular dip on its computed discharge current, whereas in a PFD with high inductance, after the pinch phase and before the expanded column axial phase other instabilities manifesting anomalous plasma resistances could also occur leading to produce further dips on the discharge current. These dips on the discharge current are called the extended dips [27]. Generally, the low constant inductance systems would have a large regular dip (in depth and in time) which can easily disappear the effects of the small extended dips (in depth and in time). On the other hand, the high constant inductance systems would have a large extended dip (in both depth and time) in comparison with its small regular dip.

3.5 Expanded column axial phase

Eventually, the plasma pinch disrupts due to the onset of $m = 0$ instability. After disintegration of the pinch, a very large and hot cloud of plasma is formed, while the rest of the capacitor energy is completely discharging through it. The very large and expanded plasma causes the plasma resistance to decrease from R_{pinch} down to a negligible value around the $R_{\text{breakdown}}$ [38]. During the plasma expansion, the plasma inductance is still increasing, but with a steepness almost similar to the axial phase. In this case, during the next half-period, the plasma inductance in this phase can assign a value from 3 to 5 nH as the simulation input.

In order to determine the range of the constant inductance, it can be used the principle of the maximum power transmission in the PFDs. It has been reported [47] that one of the important design parameters is the good matching between the external inductance and plasma inductance ($L_{\text{ext}} \approx L_p$). In practice, if this condition is fulfilled, the efficiency of the PFD will be maximized. Therefore, regarding to the total inductance of plasma, the constant inductance can be estimated to be about from 21 to 29.5 nH.
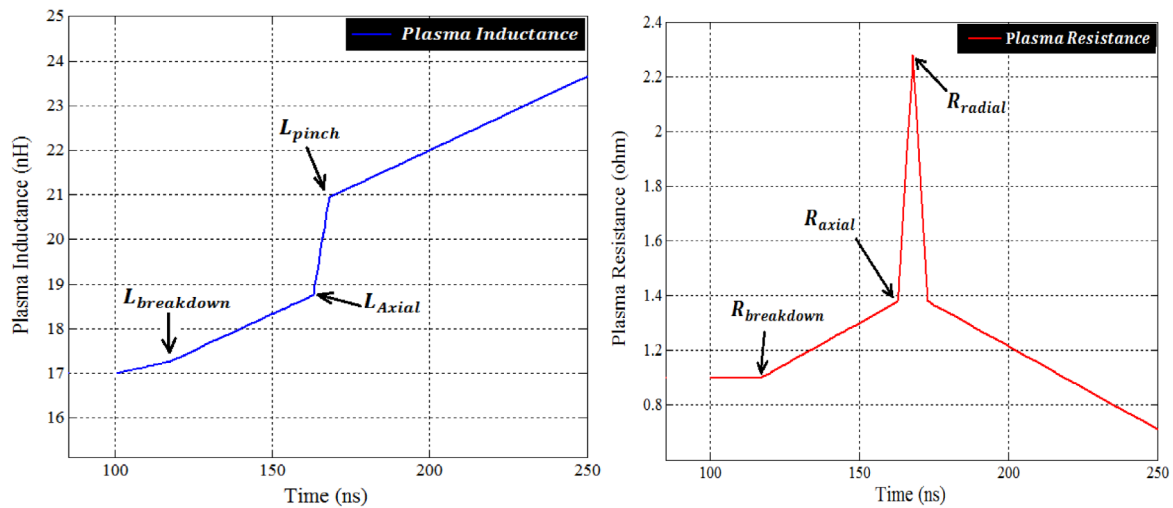
Fig. 2. The signals of the plasma inductance and plasma resistance inserted into the simulation as inputs and plotted by SIMULINK.
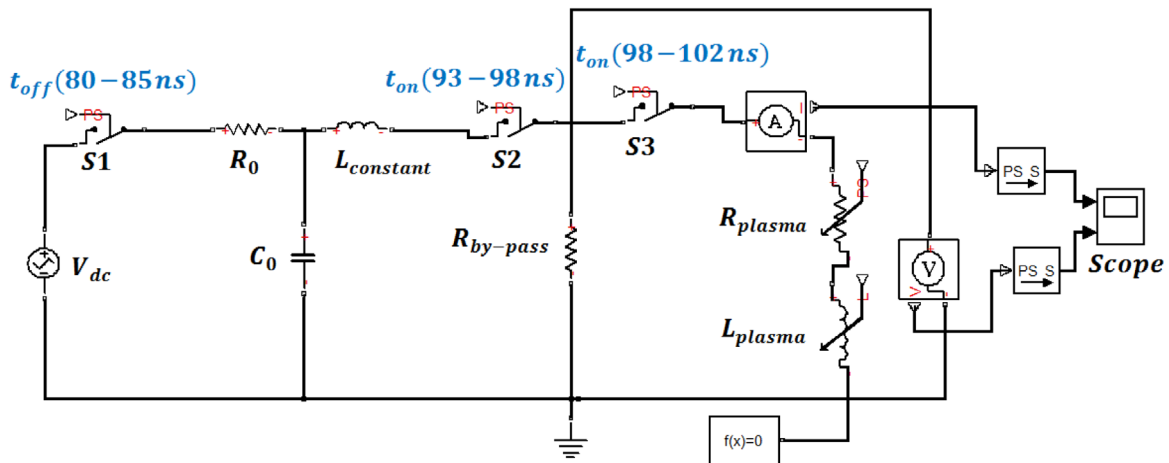

Fig. 3. The equivalent discharge circuit of the PFD that has been modeled and then simulated in SIMULINK.

To simulate the equivalent discharge circuit of the PFD in SIMULINK, the variation of inductances described for plasma dynamics phases should be inserted in simulation as the inputs. The inductance of each phase is defined in SIMULINK by means of two Ramp Function Blocks. An Add Block gathers the values of the Ramp Function Blocks and then it is connected to the Variable Inductor by means of a Simulation-PS Convertor Block to create the signal of the plasma inductance. The function of the Variable Inductor has been defined based on equation of $V_L(t) = L(t)[di(t)/dt] + i(t)[dL(t)/dt]$. Thus, by applying the signal of the plasma inductance to the Variable Inductor, both terms $[di(t)/dt]$ and $[dL(t)/dt]$ are appeared during the simulation. The signal of the plasma resistance has a more simple equation instead of the plasma inductance as $V_R(t) = R(t)i(t)$ which is of course defined similarly to way of the plasma inductance and it is finally applied to a Variable Resistor. The signals of the plasma resistance and plasma inductance inserted into the simulation as inputs and plotted by SIMULINK are displayed in Figure 2. In accordance to Figure 2, the plasma dynamics begins after

100 ns from running the simulation. The simulated circuit of the PFD discharge is observed in Figure 3. As shown in Figure 3, the discharge circuit has been completed by adding a charging voltage circuit.

4 Simulation results and discussion

A PFD operating at the energy of 3.6 J has been designed. The charging voltage of 15 kV is supplied by a switching power supply along with a rechargeable battery (12 V dc, 24 A h) that allows the device to be a compact and portable system. The electrical and geometrical parameters of the system have been listed in Table 1.

In order to have a clear insight into the discharge mechanism of the PFD, we have also provided a new model for simulating the discharge circuit of the very small PFD, having ability to investigate the effect of variation at each parameter.

The most important parameter of a PFD is the inductance so that its value can change by modifying the
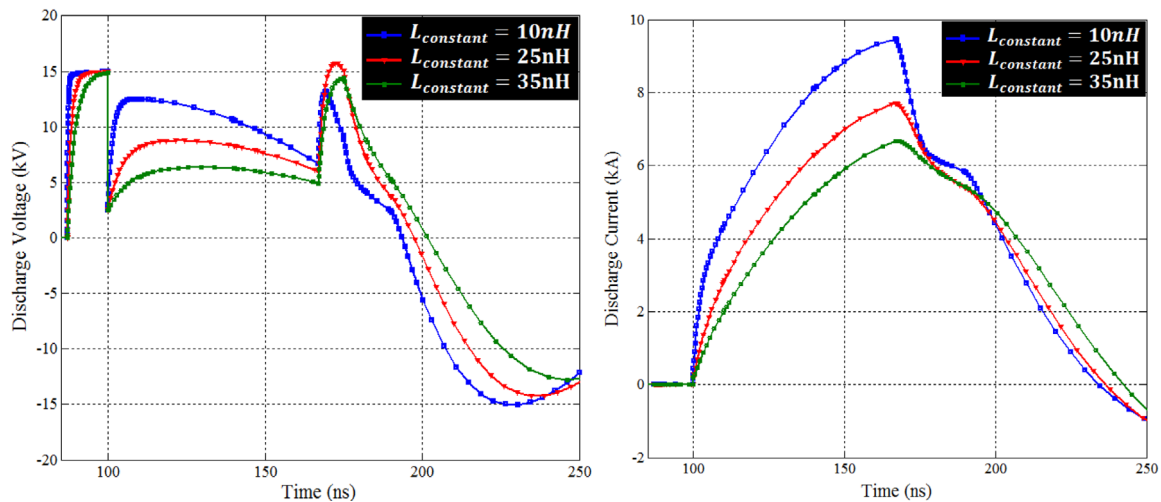
Fig. 4. The signals of discharge voltage and discharge current as the simulation results for the constant inductances of 10 nH, 25 nH, and 35 nH.

dimensions of electrodes and other geometrical parameters of the device. Since the plasma inductance is related to the dimensions of electrodes which have been calculated before and are then certain, so we just ran the simulation by considering the variation of two other important inductances, i.e. the constant inductance and the inductance of the breakdown phase that is related to the size of vacuum chamber that includes the electrodes and insulator.

Before the beginning of the breakdown phase, a magnetic energy has been stored in the constant inductance, so the effectiveness of the constant inductance on the operation of the PFD is more than the plasma inductance. However, the formation of the pinch is occurred due to the instantaneous and substantial variation of the plasma inductance. Therefore, the constant inductance can assign a high value while it does not neutralize the effect of plasma inductance variation.

If the constant inductance becomes very higher than the variable inductance, the reduction of the discharge current during the pinching takes more time that is due to the increment of the time constant, thus this event leads to produce a defective pinch. As mentioned above, this typical current dip is observed on the discharge current signals of PFDs with high constant inductance that is called an extended dip [27]. On the other hand, if the constant inductance becomes much less than the variable inductance, during the pinching the discharge current will have an intense dip. Hence, a very low energy is transferred to the plasma that causes the formed pinch to become again very weak. This event occurs in PFDs with low constant inductance observing a regular dip on their discharge current signals [27]. Figure 4 shows the signals of discharge voltage and discharge current as simulation results for constant inductances of 10 nH, 25 nH, and 35 nH and the breakdown inductance of 17 nH. As shown in Figure 4, for inductance of 10 nH, a quick rise has been created on the current signal which is due to the decrease of the impedance at the moment of discharge. For this system with low constant inductance of 10 nH, it can be seen a regular dip region

with large depth and duration of about 10 ns on the discharge current as it was expected. The voltage signal has also obtained a very low amplitude, indicating to create a weak pinch. By increasing the inductance up to 25 nH, an appropriate pinch has been created, leading to increase in system's efficiency. This inductance along with the about 1 Ω pinch resistance have caused the voltage spike to obtain a sharper peak with a higher amplitude. Those are also what cause the appropriate dip on the discharge current [27]. When the constant inductance becomes about 35 nH, despite of creation of a appropriate voltage spike, the amplitude of the discharge current will become low because of increment of the system impedance. Furthermore, the time constant also increases which causes the discharge current to take more time to decrease. Therefore as it was expected, for this system with high constant inductance of 35 nH, a high scale extended dip region can be seen with a large timescale of about 25 ns on the discharge current.

It is also seen that during the breakdown phase to the acceleration phase, the constant inductance of 25 nH has led to create a smooth trace of discharge voltage completely similar to the experimental traces of discharge voltage that are presented in published literatures [16,18,19,35]. This event is due to the appropriate value of plasma inductance variation in the presence of the constant inductance of 25 nH. The smooth voltage created before the pinch phase assists to induce a sharp spike during the pinching. Thus, the inductance of 25 nH can be specified in the designed device as the optimum constant inductance.

The inductance of the breakdown phase is related to a part of anode surrounded by insulator, anode and cathode plates. If the inductance of the breakdown phase assigns a value less than optimum value, after the breakdown occurs, the amplitude of discharge current will be increased due to the reduction of system impedance. On the other hand, since the breakdown inductance is low, the variation of plasma inductance during the pinching will be
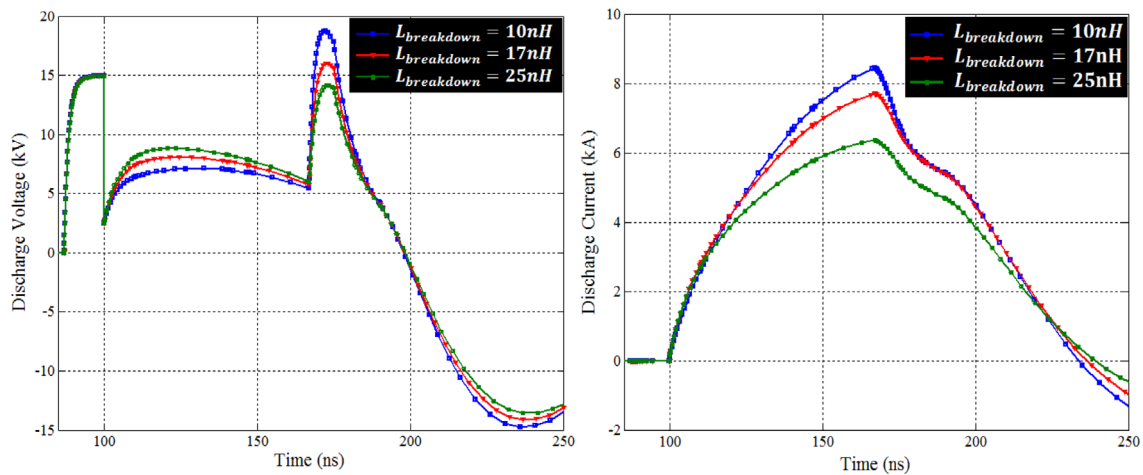
Fig. 5. The signals of discharge voltage and discharge current as the simulation results for the breakdown inductances of 10 nH, 17 nH and 25 nH.
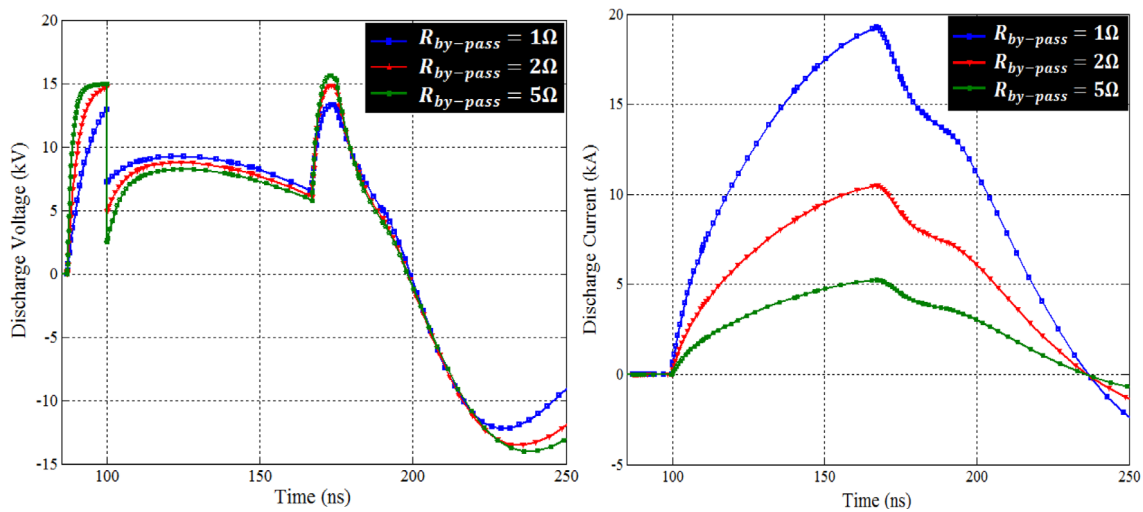

Fig. 6. The signals of discharge voltage and discharge current as the simulation results for the by-pass resistances of 1 Ω, 2 Ω and 5 Ω.

so remarkable that a sharp spike is created on the signal of discharge voltage. Figure 5 displays the signals of discharge voltage and discharge current as simulation results for the breakdown inductances of 10 nH, 17 nH and 25 nH and the constant inductance of 25 nH. As shown in Figure 5, during the pinching, for inductance of 10 nH, an intense dip has been appeared in the discharge current, and the pinch voltage also has achieved a high rise in its amplitude. Since the energy transferred to the plasma is proportional to the pinch voltage, so this high rise of the voltage spike will increase the energy transferred to the plasma, leading to produce a high yield of X-ray and neutron emission. However, the design of the chamber was so that the breakdown inductance could assign values from 15 to 25 nH. It can be seen in Figure 5 that for inductances greater than of 10 nH, the amplitudes of the pinch voltage and discharge current are a little dropped.

The comparison between simulation results and discharge voltage signals of constructed PFDs that have been presented in published literatures [16,18,19,35] express

that the values obtained for the breakdown and constant inductances are consistent with the reality, because every experimental signal of discharge voltage has an intense drop at the moment of beginning of the discharge (similar to the output voltage signal for the constant inductances between 10 and 25 nH) and also has a low pinch voltage (similar to the output voltage signal for the breakdown inductances between 17 to 25 nH). Since we intend to achieve the good pinch voltage, it can be assumed an inductance of about 10 to 17 nH as the breakdown inductance for beginning the design. However, in practice, it is a challenge getting to a very special design for reducing the inductance. So, in order to have a design that is consistent with reality, it can be reasonable to consider an inductance about 17 nH as the breakdown inductance.

In order to perceive the effectiveness of the by-pass resistance on the discharge signals, the simulation was also run with different values of resistance. Figure 6 shows the signals of discharge voltage and discharge current for by-pass resistances of 1 Ω, 2 Ω and 5 Ω. It can be seen in

Table 3. The values of parameters that were used in the simulation as input values.

| Symbol	Parameter	Value
V_{dc}	Charging voltage (kV)	15
C_0	Capacitor bank capacitance (nF)	32
R_0	Current limiter resistance (mΩ)	50
$t_{breakdown}$	Duration of the breakdown phase (ns)	18
$L_{breakdown}$	Inductance variation during the breakdown phase (nH)	17
t_{axial}	Duration of the axial acceleration phase (ns)	48
L_{axial}	Inductance variation during the axial acceleration phase (nH)	1.6
t_{radial}	Duration of the radial collapse phase (ns)	5.1
L_{radial}	Inductance variation during the radial collapse phase (nH)	2.3
$L_{expansion}$	Duration of the expanded column phase (nH)	3
$L_{constant}$	Constant inductance (nH)	25
R_{bypass}	By-pass resistance (Ω)	2.2
R_{plasma}	Plasma resistance (Ω)	1.1−2.5
S1	Switch1 (ns)	80−85
S2	Switch2 (ns)	93−98
S3	Switch3 (ns)	98−102
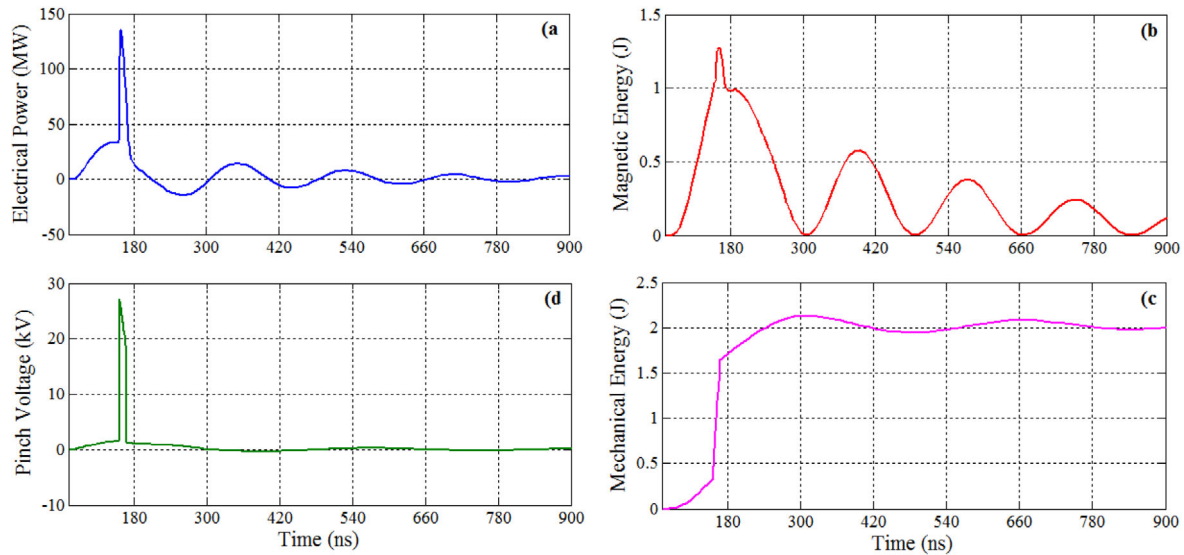
Fig. 7. Other electrical characteristics obtained from simulation for the 3.6J PFD (a) electrical power; (b) magnetic energy; (c) mechanical energy; (d) pinch voltage.

Figure 6 that each increment in the by-pass resistance causes to create a higher pre-breakdown voltage with a short rise time. This event is due to the increment of the discharge current during the pre-breakdown phase that is flowing through the by-pass resistance. It should be also mentioned that at the moment of discharge, a small by-pass resistance causes the voltage signal to begin from a higher amplitude of voltage. As shown in Figure 6, if the by-pass resistance assigns values less than the calculated resistance of 2.28 Ω, the discharge current will becomes very greater than discharge peak current. In this case, this very low resistance cannot be the expected leakage resistance. The expected discharge current for by-pass resistance of 2.28 Ω is about 7 kA. For by-pass resistance of 2 Ω, it is obvious that the discharge current has been reached to the expected amplitude. Table 3 gives the values of

the parameters that were used in the simulation as input values.

Further investigations carried out on the model showed for achieving a good pinch in the PFD, the total inductance of the system should be low, but there is an optimum inductance which helps to reach an appropriate pinch.

The other electrical characteristics of the very small PFD obtained from the simulation have been shown in Figure 7. The total electrical power which is transferred into the whole plasma system (includes the powers transferred into the plasma and the magnetic field outside of plasma) is obtained from multiplying discharge voltage by discharge current. As shown in Figure 7a, a very large electrical power of around 140 MW has been produced by the pulsed power supply, for energizing the very small PFD of 3.6 J. This graph demonstrates the ability of the pulsed

power supplies in producing the high and instantaneous electrical power. The compression of the plasma is carried out by the energy stored into the inductance of the system, called the magnetic energy. This energy is given by:

$$E_{\mathrm{mag}} = \frac{1}{2} L_p I_{\mathrm{dis}}^2 \qquad (6)$$

where L_p and I_{dis} are plasma inductance and discharge current respectively. As shown in Figure 7b, the magnetic energy has a high growth up to 1.3 J during the pinching which is due to the maximum discharge current. A part of the maximum energy which has been stored into the plasma is converted into the mechanical energy. In the final phase, the radial speed which has been produced by the mechanical energy assists the magnetic energy to create a very dense plasma column. Figure 7c shows the signal of the mechanical energy that is given by:

$$E_{\mathrm{mech}} = \frac{1}{2} \int_0^t I_{\mathrm{dis}}^2 \frac{dL_p}{dt} dt. \qquad (7)$$

The mechanical energy at the end of the acceleration phase has been obtained about 1.6 J. It should be mentioned that some of the total energy of the capacitor bank has been lost by the plasma resistance. Another important parameter is the pinch voltage that distinguishes the power of pinching. The pinch voltage is calculated by:

$$V_{\mathrm{pinch}} = \left(\frac{dL_p}{dt} \right) I_{\mathrm{dis}} + R_p I_{\mathrm{dis}} \qquad (8)$$

where R_p is the plasma resistance. Refer to (4), during the pinching, due to the creation of a very high positive variation in inductance, the voltage grows very fast up to about twofold. By comparing (3) and (4), it is observed that the energy has a direct relation with the pinch voltage. Hence, every increment in the pinch voltage will increase the energy, leading to development of the pinch. Figure 7d shows the pinch voltage signal. The maximum of the pinch voltage has been seen to be about 28 kV.

There are some studies and reports about estimating the pinch resistance and its effects on the current dip in PFDs with high constant inductance [26,27,48], however the presented technique here can especially be developed and improved for investigating the effects of the plasma resistance in PFDs with high constant inductance during and after the pinch phase on the current dip too.

5 Conclusion

A novel technique was presented for obtaining the better insight into the discharge mechanism of the PFDs. The technique was based on a correlation between the electrical discharge circuit and plasma dynamics in the PFDs. This method employed the electrical and geometrical parameters of a very small PFD which designed operating at the energy of 3.6 J as the input parameters of the simulation. The input values of the simulation included the charging

voltage, capacitor bank capacitance, current limiter resistance, by-pass resistance as well as the time-dependent inductance and resistance of the plasma sheath which were calculated by assuming the plasma dynamics as transit times in going from one phase to the next. By studying the simulation results, the optimum constant inductance and optimum breakdown inductance were specified to be 25 nH and 17 nH respectively, leading to create an appropriate pinch and consequently increasing the system's efficiency. This optimum inductance along with the about 1 Ω pinch resistance caused to create a sharp rise on the voltage signal and an appropriate dip on the discharge current, demonstrating a good agreement between the model and the experiments. The model also demonstrated for achieving a good pinch in the PFD, the total inductance of the system should be low; however there is always an optimum inductance which gives an appropriate pinch. The simulation results also showed an electrical power of about 140 MW produced by the pulsed power supply for energizing the 3.6 J PFD. The mechanical and magnetic energies assigned values about 1.6 J and 1.3 J respectively; and the pinch voltage reached to a value around 28 kV.

References

1. N. Filippov, T. Filippova, V. Vinogradov, Nucl. Fusion Suppl. **2**, 577 (1962)
2. J.W. Mather, Phys. Fluids **8**, 366 (1965)
3. L. Soto, P. Silva, J. Moreno, M. Zambra, W. Kies, R.E. Mayer, A. Clausse, L. Altamirano, C. Pavez, L. Huerta, J. Phys. D **41**, 205215 (2008)
4. L. Soto, P. Silva, J. Moreno, G. Silvester, M. Zambra, C. Pavez, L. Altamirano, H. Bruzzone, M. Barbaglia, Y. Sidelnikov, W. Kies, Braz. J. Phys. **34**, 1814 (2004)
5. M. Scholz, R. Miklaszewski, M. Paduch, M.J. Sadowski, A. Szydlowski, K. Tomaszewski, Plasma Sci. IEEE Trans. **30**, 476 (2002)
6. E.J.T. Burns, S.M. Falacy, R.A. Hill, P.D. Thacher, H.A. Koehler, B. Davis, R.E. Shafer, Phys. Lett. A **133**, 144 (1988)
7. G. Verri, F. Mezzetti, A. Da Re, A. Bertolotti, L. Rapezzi, V. Gribkov, Nukleonika **45**, 189 (2000)
8. V.A. Gribkov, I.V. Volobuev, Nukleonika **45**, 185 (2000)
9. M. Milanese, R. Moroso, J. Pouzo, Eur. Phys. J. D **27**, 77 (2003)
10. L. Rapezzi, M. Angelone, M. Pillon, M. Rapisarda, E. Rossi, M. Samuelli, F. Mezzetti, Plasma Sources Sci. Technol. **13**, 272 (2004)
11. T. Kobata, Plasma Phys. Control. Fusion **26**, 575 (2000)
12. S. Lee, T.Y. Tou, S.P. Moo, M.A. Eissa, A.V. Gholap, K.H. Kwek, S. Mulyodrono, A.J. Smith, Suryadi, W. Usada, M. Zakaullah, Am. J. Phys. **56**, 62 (1988)
13. F. Beg, K. Krushelnick, C. Gower, S. Torn, A. Dangor, A. Howard, T. Sumner, A. Bewick, V. Lebedenko, J. Dawson, Appl. Phys. Lett. **80**, 3009 (2002)
14. L. Soto, C. Pavez, M. Zambra, J. Moreno, A. Clausse, M. Barbaglia, *Nanofocus: An Ultra Miniature Pinch Focus Discharge Operating at 0.1 Joule* (2005), pp. 1368–1371
15. R.K. Rout, P. Mishra, A.M. Rawool, L.V. Kulkarni, C.G. Satish, J. Phys. D **41**, 205211 (2008)

16. P. Silva, J. Moreno, L. Soto, L. Birstein, R.E. Mayer, W. Kies, Appl. Phys. Lett. **83**, 3269 (2003)
17. M. José, S. Patricio, S. Leopoldo, Plasma Sources Sci. Technol. **12**, 39 (2003)
18. S. Patricio, S. Leopoldo, K. Walter, M. José, Plasma Sources Sci. Technol. **13**, 329 (2004)
19. S.M. Hassan, T. Zhang, A. Patran, R.S. Rawat, S.V. Springham, T.L. Tan, D. Wong, W. Wang, S. Lee, V.A. Gribkov, S.R. Mohanty, P. Lee, Plasma Sources Sci. Technol. **15**, 614 (2006)
20. P. Silva, L. Soto, J. Moreno, G. Sylvester, M. Zambra, L. Altamirano, H. Bruzzone, A. Clausse, C. Moreno, Rev. Sci. Instrum. **73**, 2583 (2002)
21. L. Soto, A. Esaulov, J. Moreno, P. Silva, G. Sylvester, M. Zambra, A. Nazarenko, A. Clausse, Phys. Plasmas **8**, 2572 (2001)
22. S. Lee, P. Lee, S.H. Saw, R.S. Rawat, Plasma Phys. Control. Fusion **50**, 065012 (2008)
23. S. Lee, S.H. Saw, Energies **3**, 711 (2010)
24. M. Akel, Sh. Al-Hawat, S. Lee, J. Fusion Energy **29**, 94 (2010)
25. S. Lee, S.H. Saw, Appl. Phys. Lett. **92**, 021503 (2008)
26. V. Felipe, T.-S. Ariel, P. Cristian, M. José, Z. Marcelo, S. Leopoldo, Plasma Phys. Control. Fusion **54**, 095007 (2012)
27. S. Lee, S.H. Saw, A.E. Abdou, H. Torreblanca, J. Fusion Energy **30**, 277 (2011)
28. J. Mather, Meth. Exp. Phys. **9**, 187 (1971)
29. S. Lee, A. Serban, IEEE Trans. Plasma Sci. **24**, 1101 (1996)
30. T. Zhang, R.S. Rawat, S.M. Hassan, J.J. Lin, S. Mahmood, T.L. Tan, S.V. Springham, V.A. Gribkov, P. Lee, S. Lee, IEEE Trans. Plasma Sci. **34**, 2356 (2006)
31. A. Bernard, H. Bruzzone, P. Choi, H. Chuaqui, V. Gribkov, J. Herrera, K. Hirano, A. Krejci, S. Lee, C. Luo, J. Moscow Phys. Soc. **8**, 93 (1998)
32. T. Zhang, X. Lin, K. Chandra, T. Tan, S. Springham, A. Patran, P. Lee, S. Lee, R. Rawat, Plasma Sources Sci. Technol. **14**, 368 (2005)
33. M. Zakaullah, I. Ahmad, A. Omar, G. Murtaza, M. Beg, Plasma Sources Sci. Technol. **5**, 544 (1999)
34. A. Donges, G. Herziger, H. Krompholz, F. Rühl, K. Schönbach, Phys. Lett. A **76**, 391 (1980)
35. R.K. Rout, A.M. Rawool, L.V. Kulkarni, T.C. Kaushik, S.C. Gupta, in *Proc. of 16th Annual Conference of Indian Nuclear Society, Mumbai, India, 2005*, Vol. 16
36. M.S. Rafique, Ph.D. thesis National Institute of Education, Nanyang Technological University in fulfilment of the requirement for the degree of Doctor of Philosophy, Singapore, 2000
37. H.R. Yousefi, F.M. Aghamir, K. Masugata, Phys. Lett. A **361**, 360 (2007)
38. S. Lee, S. Saw, *Joint ICTP-IAEA Workshop on Dense Magnetized Plasma and Plasma Diagnostics* (2010)
39. V. Rishi, M.V. Roshan, F. Malik, P. Lee, S. Lee, S.V. Springham, T.L. Tan, M. Krishnan, R.S. Rawat, Plasma Sources Sci. Technol. **17**, 045020 (2008)
40. L. Soto, J. Moreno, P. Silva, C. Pavez, M. Cárdenas, L. Altamirano, *2nd Research Coordination Meeting of AIEA CRP on Neutron Based Techniques for the Detection of Illicit Materials and Explosives, Mumbai, India, 2007*
41. S. Leopoldo, P. Cristian, M. José, B. Mario, C. Alejandro, Plasma Sources Sci. Technol. **18**, 015007 (2009)
42. S. Lee, IEEE Trans. Plasma Sci. **19**, 912 (1991)
43. N. Georgescu, J. Larour, V. Zoita, in *Pulsed Power'96, IEE Colloquium on* (1996), pp. 32/1-32/3
44. S. Lee, S.H. Saw, in *Joint ICTP-IAEA Workshop on Dense Magnetized Plasma and Plasma Diagnostics, Trieste, Italy, 2010*
45. S.H. Saw, P.C.K. Lee, R.S. Rawat, S. Lee, Plasma Sci. IEEE Trans. **37**, 1276 (2009)
46. L. Mahe, F. Xianping, S.V. Springham, L. Sing, Plasma Sci. IEEE Trans. **26**, 135 (1998)
47. A. Talaei, S. Sadat Kiai, J. Fusion Energy **28**, 304 (2009)
48. R. Verma, R.S. Rawat, P. Lee, M. Krishnan, S.V. Springham, T.L. Tan, IEEE Trans. Plasma Sci. **38**, 652 (2010)